Microvascular Research 146 (2023) 104456

Contents lists available at ScienceDirect

Microvascular Research

journal homepage: www.elsevier.com/locate/ymvre

Flowmotion imaging analysis of spatiotemporal variations in skin microcirculatory perfusion

Martin Hultman [a,b,*], Marcus Larsson [a], Tomas Strömberg [a], Joakim Henricson [c,d], Fredrik Iredahl [e,f], Ingemar Fredriksson [a,b]

[a] Department of Biomedical Engineering, Linköping University, Sweden
[b] Perimed AB, Datavägen 9A, Järfälla, Stockholm, Sweden
[c] Department of Emergency Medicine, Region Östergötland, Linköping, Sweden
[d] Department of Biomedical and Clinical Sciences, Linköping University, Linköping, Sweden
[e] Division of Community Medicine, Department of Health, Medicine and Caring Sciences, Linköping University, Linköping, Sweden
[f] Department of Primary Health Care, Region Östergötland, Linköping, Sweden

ARTICLE INFO

Keywords:
Flowmotion
Vasomotion
Microcirculation
Perfusion
MELSCI
LSCI

ABSTRACT

Background: Flowmotion is the rhythmical variations in measured skin blood flow that arise due to global and local regulation of the vessels and can be studied using frequency analysis of time-resolved blood flow signals. It has the potential to reveal clinically useful information about microvascular diseases, but the spatial heterogeneous nature of the microvasculature makes interpretation difficult. However, recent technological advances in multi-exposure laser speckle contrast imaging (MELSCI) enable new possibilities for simultaneously studying spatial and temporal variations in flowmotion.
Aim: To develop a method for flowmotion analysis of MELSCI perfusion images. Furthermore, to investigate the spatial and temporal variations in flowmotion in forearm baseline skin perfusion.
Method: In four healthy subjects, forearm skin perfusion was imaged at 15.6 fps for 10 min in baseline. The time-trace signal in each pixel was analyzed using the wavelet transform and summarized in five physiologically relevant frequency intervals, resulting in images of flowmotion. Furthermore, a method for reducing the effect of motion artifacts in the flowmotion analysis was developed.
Results: The flowmotion images displayed patterns of high spatial heterogeneity that differed between the frequency intervals. The spatial variations in flowmotion, quantified as the coefficient of variation, was between 11 % and 31 % in four subjects. Furthermore, significant temporal variations in flowmotion were also observed, indicating the importance of a spatiotemporal analysis.
Conclusion: The new imaging technique reveals significant spatial differences in flowmotion that cannot be obtained with single-point measurements. The results indicate that global statistics of flowmotion, such as the mean value in a large region of interest, is more representative of the microcirculation than data measured only in a single point. Therefore, imaging techniques have potential to increase the clinical usefulness of flowmotion analysis.

1. Introduction and aim

A normal and healthy microcirculation is characterized by the ability to match tissue needs of adequate delivery of nutrients and oxygen, while enabling removal of waste products (Ellis et al., 2005). By changes in network conductance, affected by regulatory activity of myogenic, neurogenic, and endothelial mechanisms, tissue needs can be satisfied. The oscillatory pattern of changes in arteriolar diameter, observed by frequency analysis, is known as vasomotion, and the resulting oscillations in blood flow are called flowmotion (Rossi et al., 2006a). Obesity and insulin resistance (Clough et al., 2017), and peripheral arterial disease (Rossi et al., 2005), to name just a few examples, have been suggested to be potential areas where flowmotion analysis could reveal aspects of clinical importance. The endothelial dysfunction observed in sepsis, affecting vasoregulation, barrier function, and inflammation, is another potential area (Ince et al., 2016). However, previous studies

* Corresponding author at: Department of Biomedical Engineering, Linköping University, Sweden.
E-mail address: martin.o.hultman@liu.se (M. Hultman).

https://doi.org/10.1016/j.mvr.2022.104456
Received 20 September 2022; Received in revised form 2 November 2022; Accepted 12 November 2022
Available online 18 November 2022

have so far not led to a consensus in the scientific community regarding the clinical usefulness of flowmotion analysis. This can partially be explained by the spatial and temporal variations in skin microcirculation (Wardell et al., 1994) in conjunction with the use of single-point measurement techniques.

So far, laser Doppler flowmetry (LDF) has been the method of choice for studies of flowmotion, although newly developed measurement techniques enable further physiological aspects to be explored. In a recent study, we used Periflux 6000 EPOS (Perimed AB, Järfälla, Stockholm, Sweden) to analyze flowmotion from speed-resolved perfusion, as well as variations in red blood cell tissue fraction, oxygen saturation, and vessel diameter (Fredriksson et al., 2022). By applying magnitude scalograms and time-averaged wavelet spectra, recurring periods of intensified energy could be observed within each frequency interval, which highlights the potential of temporal variations.

LDF is limited to single-point measurements, which might lead to large variations in the computed flowmotion depending on the probe placement. Laser speckle contrast imaging (LSCI) instead records blood flow images, which can reveal these spatial variations. Recently, it was demonstrated that the flowmotion temporal variations in regions-of-interest from LSCI perfusion images correlate well with LDF (Mizeva et al., 2020), indicating that analysis methods developed for LDF can be extended to LSCI. However, despite the spatial nature of LSCI, the authors did not provide spatial maps of flowmotion activity, possibly due to the higher susceptibility to noise in LSCI compared to LDF (Fredriksson and Larsson, 2016). We have recently developed a new perfusion imaging technique based on a combination of multi-exposure laser speckle contrast imaging (MELSCI) and a machine learning model that enables continuous imaging of skin perfusion at 15.6 fps with accuracy equal to LDF, as well as lower susceptibility to measurement noise than LSCI (Fredriksson et al., 2019; Hultman et al., 2020). Thus, by applying the flowmotion analysis methods previously developed for LDF, individually in each pixel, the new MELSCI perfusion technique enables the observation of high-resolution spatial and temporal variations in skin flowmotion.

The aim of this study is to present a method for calculating flowmotion images based on MELSCI and LSCI perfusion. Furthermore, we study the spatial and temporal flowmotion variations in skin perfusion in baseline conditions.

2. Method

2.1. Measurement system

The MELSCI system used in this study has been rigorously described in previous publications (Fredriksson et al., 2019; Hultman et al., 2020; Hultman et al., 2017). For this paper however, it is sufficient to understand that the system acquires perfusion images at 15.6 frames per second (Hultman et al., 2020), where the perfusion is equivalent to perfusion obtained from LDF (Fredriksson et al., 2019). This is not the case in conventional single-exposure LSCI, where high perfusion is underestimated compared to LDF and by extension to true perfusion (Fredriksson and Larsson, 2016). The framerate is sufficiently high to capture the cardiac-related temporal variations in the blood flow signal.

2.2. Measurement protocol

Four healthy volunteers were acclimated in a temperature-controlled room for 20 min. Data was then collected on the volar forearm for 10 min, at a distance of 25–30 cm. A vacuum pillow was used for arm support to minimize motion artifacts. Written informed consent was given by the participants before the experiment, and all data was pseudonymized. The study protocol was approved by the Swedish Ethical Review Authority, d.no. 2019–04713.

2.3. Processing

For each participant, the measurement resulted in 9375 images of 256 × 320 pixels (10 min at 15.625 frames per second = 9375 timepoints). Two different processing pipelines were used for analysis of images and regions-of-interest (ROIs), respectively. This is summarized in Fig. 1, and explained below.

To reduce noise in the image analysis, a 5 × 5 spatial Gaussian lowpass filter with $\sigma = 1$ was applied individually to each image before further analysis. The 10-minute perfusion signal from each individual pixel was then corrected for motion artifacts, after which the magnitude scalogram was computed with the continuous wavelet transform (CWT).

2.3.1. Motion artifact removal

Motion artifacts in speckle imaging primarily present as spikes of abnormally high perfusion, usually lasting just one or a few samples. This adds high amounts of energy to the signal across the entire frequency spectrum. When computing the CWT magnitude scalograms, the affected time interval increases for decreasing frequencies, thus creating the "widening cone" artifacts seen in Fig. 2c. To remove these artifacts, we applied a 20-second (313 samples) Hampel filter as an outlier detector on the perfusion signal. Specifically, we defined outliers as samples more than 4 standard deviations from the local median in a moving 20-second window, where the standard deviation was estimated using the scaled median absolute deviation (MAD):

$$\sigma \approx 1.48 \cdot \overline{|x - \bar{x}|}, \tag{1}$$

where $\bar{x}$ denotes the median. To increase the robustness of the detection, values within 4 samples (0.25 s) of outliers were additionally defined as outliers. Detected outliers were replaced by linear interpolation between the first valid preceding and succeeding sample. Note that the median filter was only used to detect outliers. The corrected signal was not filtered. Fig. 2 illustrates this algorithm using synthetic data. The signal in (a) was generated by a sum of five random amplitude sinusoidal signals at the center of the frequency bands corresponding to the cardiac, respiratory, myogenic, neurogenic, and endothelial activity, followed by the addition of Gaussian noise. Finally, motion artifacts with random amplitude and duration were added to the signal. In real data, negative motion artifacts are rare but possible, and we therefore demonstrate that the algorithm works equally well in this case. The zoomed-in plots in the figure show the signal before and after motion artifact removal, demonstrating that most of the signal is unaffected by the algorithm. The CWT magnitude scalogram for the original signal without motion artifacts is shown in (b), and with motion artifacts in (c). The CWT scalogram after correction for motion artifacts is shown in (d). While the original signal cannot be completely reconstructed, the impact on the CWT magnitude scalogram can be significantly reduced using this method, as summarized by the relative errors in the figure titles.

2.3.2. Wavelet analysis

Several analysis methods have been proposed for flowmotion, using either the Fourier spectrum or wavelet spectrum of the blood flow signal. In addition to studying the full spectrum, the data is commonly further summarized as the sum of energy in the five frequency bands of interest. First proposed by Stefanovska et al. (Stefanovska et al., 1999), these bands reflects cardiac (1.6–0.4 Hz), respiratory (0.4–0.15 Hz), myogenic (0.15–0.06 Hz), neurogenic (0.06–0.02 Hz), and endothelial (0.02–0.0095 Hz) activity.

The motion artifact-corrected perfusion signal in each pixel in the data-cube was normalized according to

$$P_{\text{norm}} = \frac{P}{\langle P \rangle_t} - 1, \tag{2}$$

where $\langle \cdot \rangle_t$ denotes the time average. The normalization removed the dependence on perfusion magnitude and minimized spectral leakage

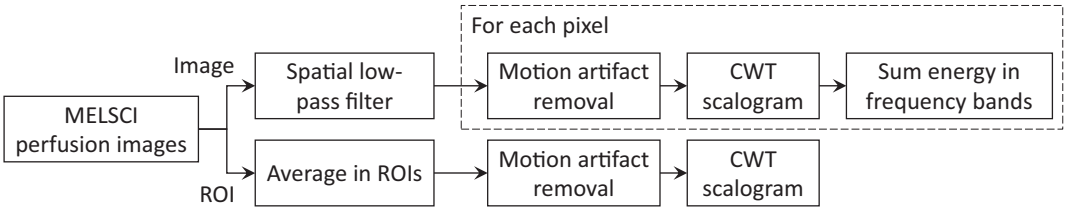

Fig. 1. Schematic overview of the processing pipeline. MELSCI = Multi-exposure laser speckle contrast imaging. CWT = Continuous wavelet transform, ROI = Region-of-interest.

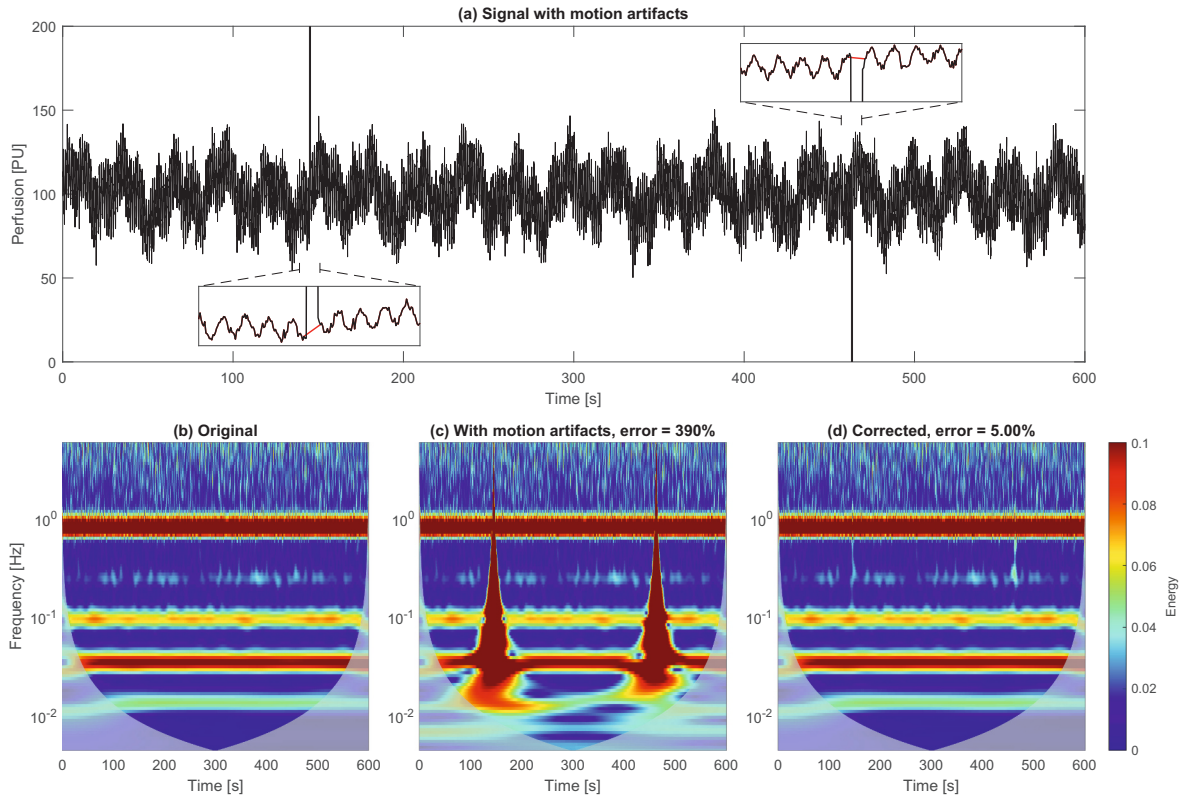

Fig. 2. Demonstration of motion artifact removal using a Hampel filter. (a) Synthetic signal with motion artifacts. Zoomed-in plots show the effect of the motion artifact correction (red graph). Note that most of the signal is unaffected by the filtering process. Zoomed-in plots span 12 s. (b) Magnitude scalogram of the original signal (no motion artifact). (c) Magnitude scalogram of the signal in (a) with motion artifacts. (d) Magnitude scalogram of the signal after motion artifact removal. The errors in (c) and (d) are the mean absolute percentage deviation in scalogram energies from the original (b).

from the DC-component of the signal (Fredriksson et al., 2022). This also resulted in the unit of the wavelet scalogram being dimensionless. However, we choose to use the term "Energy" to be consistent with nomenclature in previous publications.

The normalized signal was then transformed into a magnitude scalogram using the CWT with a Morlet wavelet using the Wavelet Toolbox in Matlab 2021b (MathWorks Inc.). The Morlet wavelet was chosen since it provides the best trade-of between time and frequency localization (Bračič and Stefanovska, 1998; Kvandal et al., 2006). The energy content in the five frequency bands were summed over the frequency dimension and averaged over the time dimension as described in Eq. (3). The result was five energy values, each representing the average energy of the five physiological processes over the 10-minute measurement. Data in the magnitude scalogram where edge effects were present due to the width of the wavelet kernel were excluded from the time average, as indicated by the gray shaded areas in the scalograms figures. The five energy values were given by

$$E_{f_L}^{f_H} = \sum_{f=f_L}^{f_H} \left(\frac{1}{F_s(t_2 - t_1)} \sum_{t=t_1}^{t_2} |\mathrm{CWT}\{P_{\mathrm{norm}}\}(f,t)| \right) \tag{3}$$

where t_1 and t_2 are the lower and upper bound of the valid time-window where edge effects in the CWT are negligible. Given the 600-second signal and Morlet wavelet, these are $t_1 = \frac{3\sqrt{2}}{\pi f}$ and $t_2 = 600 - \frac{3\sqrt{2}}{\pi f}$ seconds (Torrence and Compo, 1998) (using the default parameters for a Morlet wavelet in the Matlab 2021b Wavelet Toolbox), where f is the frequency in Hz. F_s is the sample rate, and f_L and f_H are the lower and upper frequencies of each frequency band. By applying this algorithm individually to all pixels, five flowmotion images were obtained, showing the spatial variations in the energy of the corresponding frequencies.

2.3.3. Region-of-interest analysis

In addition to the pixel-wise analysis, the scalograms were also computed in regions-of-interest (ROI). This was done using the same processing pipeline, except the spatial low-pass filter was omitted since

the spatial noise-reduction was instead performed in the ROI averaging. After computing the magnitude scalogram of the ROI signal, we also computed the frequency spectrum (time average of the scalogram) and the time-dependent variations (sum of energy in the respective frequency band for each time point) in the myogenic, neurogenic, and endothelial frequency bands.

2.3.4. Single-exposure LSCI

In addition to the results obtained from MELSCI-based perfusion, we also present results from a perfusion estimate by single-exposure LSCI as calculated in the commonly used PeriCam PSI (Perimed AB) except a slightly different exposure time:

$$P_{SE} = \frac{1}{K(8\text{ ms})} - 1, \tag{4}$$

where K is the speckle contrast as described in Refs (Hultman et al., 2020; Hultman et al., 2017).

3. Results

The results of the pixel-wise wavelet analysis summarized for each frequency band is shown in Fig. 3. These flowmotion images describe the energy content in the perfusion associated with the five physiological processes described above. The time-averaged perfusion image is also shown for comparison.

The locations of two local ROIs are marked in the images, where A and B were manually placed on locations with respective high and low activity in the three lowest frequency bands, to further highlight the spatial heterogeneity. The ROIs are circles with radius 5 pixels, thus including 81 pixels. The CWT magnitude scalograms of the ROIs are shown in Fig. 4. The frequency spectra on the right are given by the time-average of the scalograms, and the time-varying signals below the scalograms are given by the sum of energy in the respective frequency bands for each time-point.

The same type of result figures for the other three measurement subjects is given in the Supplementary material.

3.1. Single-exposure LSCI

In Figs. 5 and 6 we present the same analysis as in Figs. 3 and 4, but using perfusion estimated by single-exposure LSCI (Eq. (4)). Unlike the previous method, this perfusion estimate is not linear with respect to LDF perfusion (Fredriksson and Larsson, 2016; Fredriksson et al., 2019), but flowmotion analysis of the three lowest frequency bands yield visibly comparable results to MELSCI-based analysis. The remaining results after this section will only be presented for the MELSCI-based flowmotion analysis.

3.2. Statistical analysis of spatial variations

To understand how the spatial variations in flowmotion energy seen in Fig. 3 might impact single-point measurements such as when using LDF, we summarize the data by the histograms in Fig. 7. These show the distribution in energy in each frequency band, and illustrate the potential differences seen by different selection of measurement points. Pixels outside the large, dashed ROI in Fig. 3 were excluded to minimize the influence of edge effects from the curvature of the arm.

The spatial variations were further quantified by the coefficient of variation (CV) in the same large ROI. This was done individually for the five frequency bands and was repeated for the four subjects (Results + Supplementary). The CVs are presented in Table 1.

While these results show the variation within each frequency band, it gives no information about the variation in time-averaged spectra. Fig. 8 highlights these variations by examining the spectrum shapes in all pixels in the large ROI. Fig. 8a shows the variation in time-averaged spectra, and Fig. 8b the relative deviation from the mean spectrum. The shaded area shows the 2.5th to 97.5th percentile for each frequency, and the dashed lines show the average positive and negative deviation. The mean absolute deviation (MAD) in each frequency interval is also

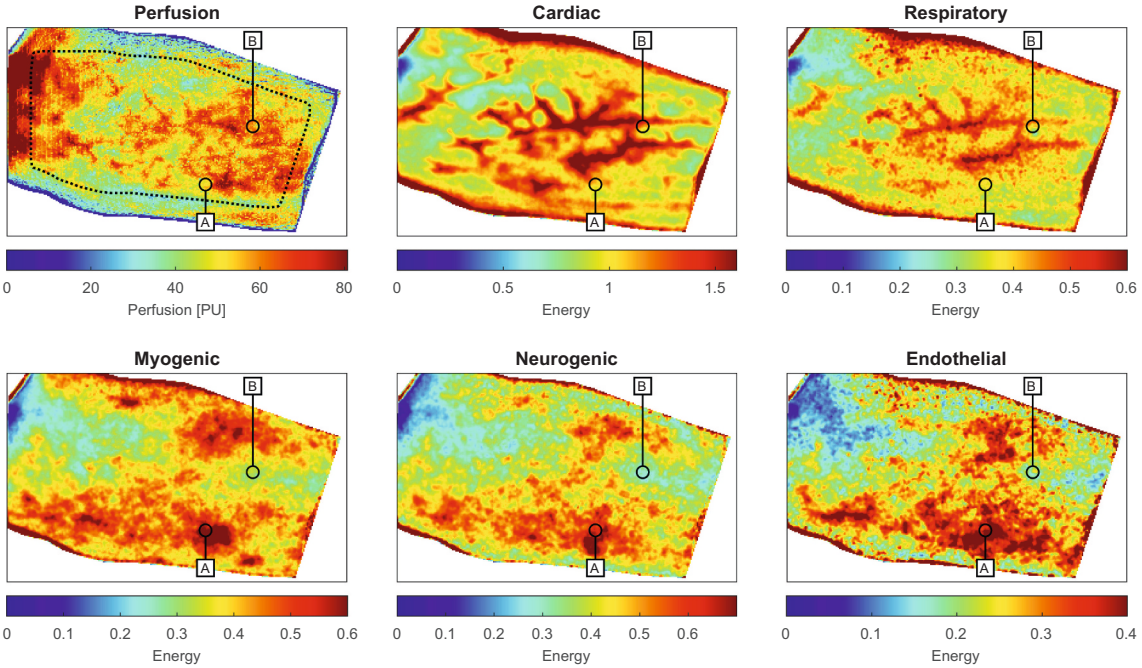

Fig. 3. Spatial variations in mean energy content in five frequency bands associated with different physiological mechanisms, as well as the mean perfusion image (top left). Image data are mean values over 600 s. The color scales were selected individually for each image to better highlight structural differences rather than the magnitude of the energy. Two regions of interest A and B are placed on areas with high respective low energy levels in the three slowest processes (myogenic, neurogenic, and endothelial). These are used for further analysis of the spatial heterogeneity (see Fig. 4). The large ROI indicated by the dotted line in the perfusion image is used for the statistical analysis of spatial variations.

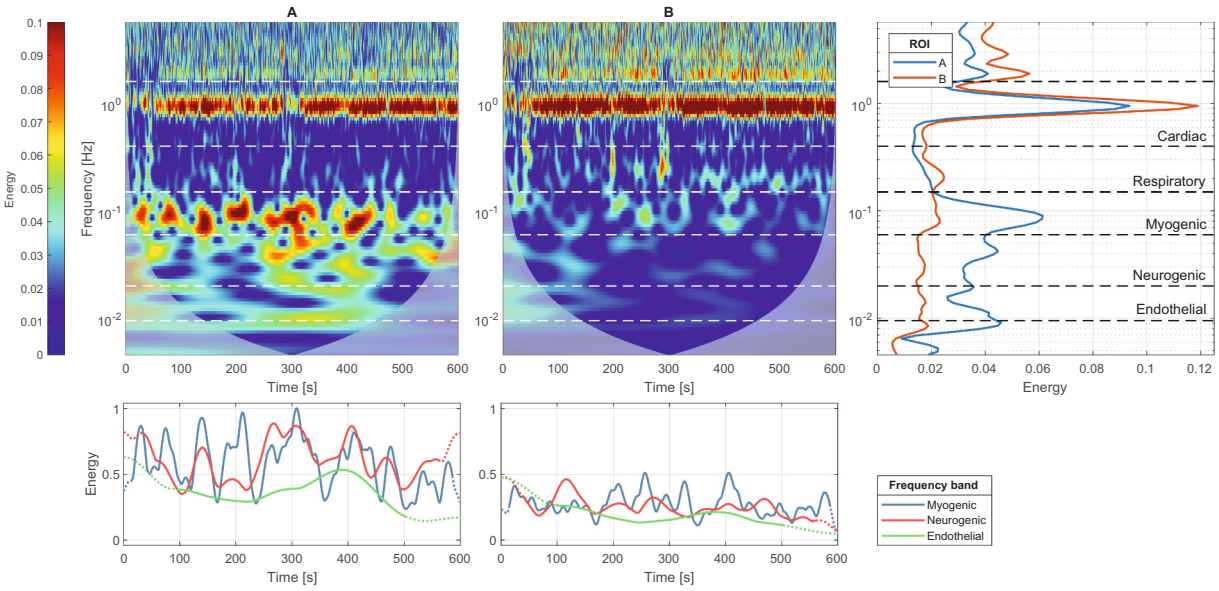

Fig. 4. Continuous wavelet transform magnitude scalograms for the two ROIs marked in Fig. 3. The rightmost plot shows the spectrogram for both ROIs averaged over the 10-minute experiment. The two lower plots show the total energy in the myogenic, neurogenic, and endothelial frequency bands as a function of time (the cardiac and respiratory frequency bands are omitted to increase visibility). The dotted line-ends in the lower plots indicate where edge effects from the CWT are significant (corresponding to the shaded area in the scalograms), and the signals should be interpreted with caution.

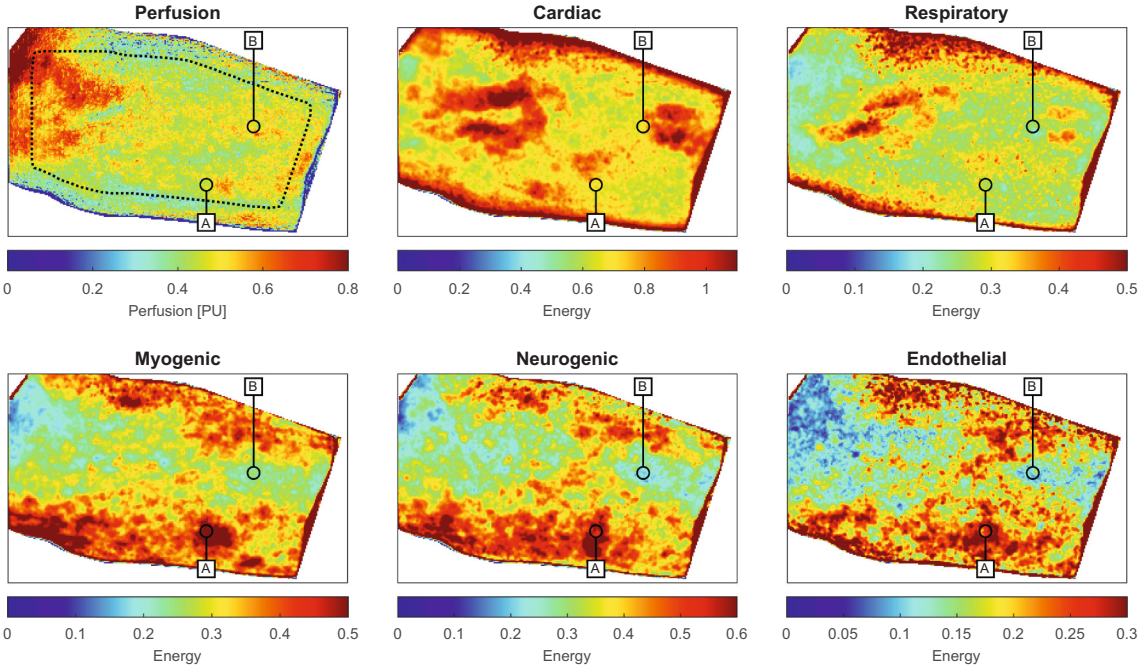

Fig. 5. Flowmotion images computed from single-exposure laser speckle contrast imaging perfusion (Eq. (4)). Image data are mean values over the 600 s data recording interval.

shown. This result demonstrates that it is on average expected to see relative differences in spectrum energies as large as 19 % compared to the mean, with 95 % confidence intervals being significantly larger.

3.3. Temporal variations in flowmotion energy

In addition to the spatial variations, we observe that flowmotion activity also changes with time, indicating increases and decreases in the activity of the various vasoregulatory mechanisms during the 10-minute measurement. These temporal variations can be significant, as shown by the flowmotion images presented at three time points in Fig. 9. The time points were selected manually to illustrate the large variations in each frequency band over time and, furthermore, that these variations are not synchronous between the different frequency intervals. At $t = 200$ s, the respiratory and myogenic energies are high, while neurogenic and endothelial energies are low. At $t = 400$ s, the respiratory energy is instead low (note also that the large vessels are no longer visible), while the myogenic, neurogenic, and endothelial energies are high. At $t = 500$ s, all four of these intervals display low energy, with some moderate activity in the myogenic interval. For cardiac energy, only slight

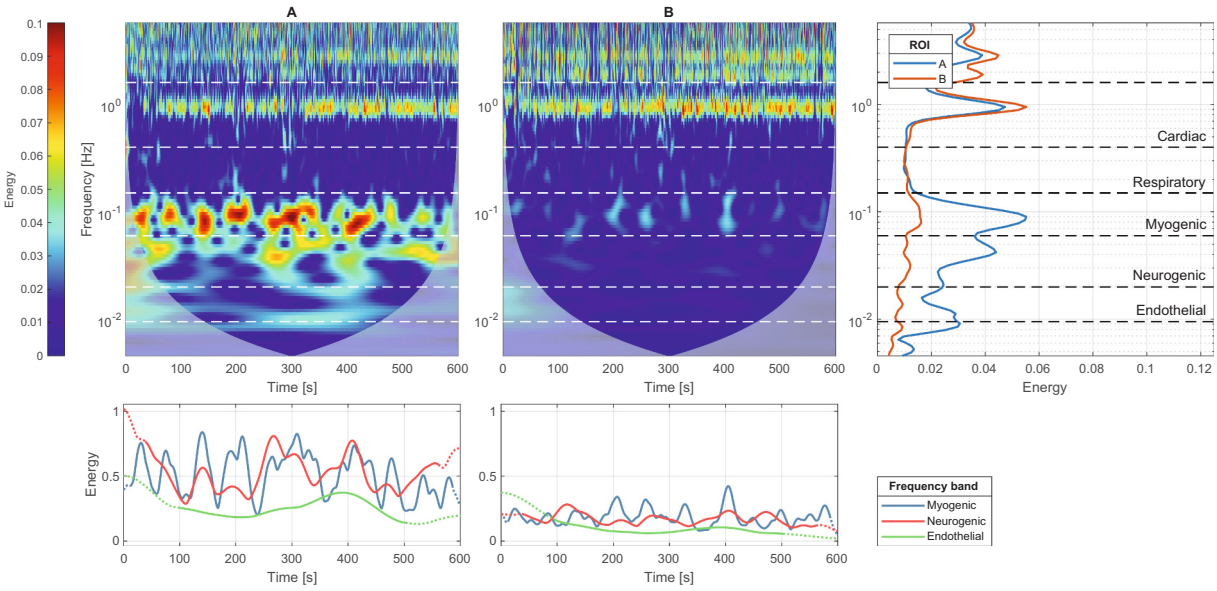

Fig. 6. Continuous wavelet transforms magnitude scalograms computed from single-exposure laser speckle contrast imaging perfusion (Eq. (4)). See Fig. 4 for an explanation of the plots.

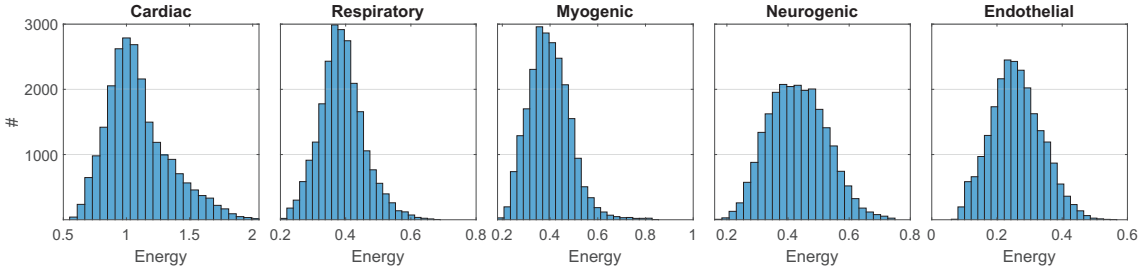

Fig. 7. Distribution of energy in the flowmotion images in Fig. 3. Only pixels within the large, dashed region of interest (Fig. 3) were included in the histogram to remove edge effects.

Table 1
Coefficient of variation [%] quantifying the spatial variation in energy over a large area of the skin (dashed ROI in Fig. 3) in four subjects. Subject 1 is presented in this main results section, subjects 2–4 are presented in the Supplementary material.

	Cardiac	Respiratory	Myogenic	Neurogenic	Endothelial
Subject 1	23	18	22	22	30
Subject 2	18	17	15	19	18
Subject 3	16	12	13	18	27
Subject 4	11	18	15	23	31

variations are visible in the selected time points. Other time points could have been chosen to illustrate larger variations, as shown in Fig. 4. However, it should be noted that the frequency of these temporal variations naturally depend of the wavelet scale at each frequency, thus cardiac variations occur rapidly.

4. Discussion

The main purpose of this paper was to develop a method for flowmotion imaging analysis from perfusion videos to reveal the magnitude of spatial and temporal variations. Our results indicate that different measurement locations can result in large variations in computed flowmotion, increasing the difficulty of finding clinical applications. As presented in Table 1, the coefficient of variation of energy in the different frequency intervals, computed in the large ROI, varied between 11 % and 31 % in the four subjects. Similarly, as presented in Fig. 8, analyzing the variations in the full spectra yields an average deviation of 19 % from the mean spectrum. Thus, to detect pathology-induced changes in the flowmotion signal, they must exceed these uncertainties to be sufficiently reliable for clinical applications. Using the image data to get the spatial information has the potential to reduce these uncertainties. It is reasonable to assume that global statistics of flowmotion, such as the mean in the large ROI, are more representative of the overall state of the microcirculation than data measured only in a single point.

Spatial variations in the wavelet spectra in a small (8 × 8 mm) tissue area have been studied previously using LSCI, specifically to investigate the respiratory variations in the blood flow signal (Mizeva et al., 2021). The most interesting comparison with our results is in the spectral variations, analogous to Fig. 8. Their analysis yielded a significantly smaller confidence interval for the spectra compared to our results in this work. This indicates that spatial variations on the small scale differs from those on the large scale seen in our images, further demonstrating the importance of measuring flowmotion in a large area to allow the use of representative measures.

Motion artifacts are one of the main weaknesses of speckle-based measurement techniques. Due to the high energy content in the artifact, it is necessary to compensate for this before applying the frequency transform. When only analyzing the perfusion signal in the time domain, it is possible to simply remove the affected samples, and methods to find

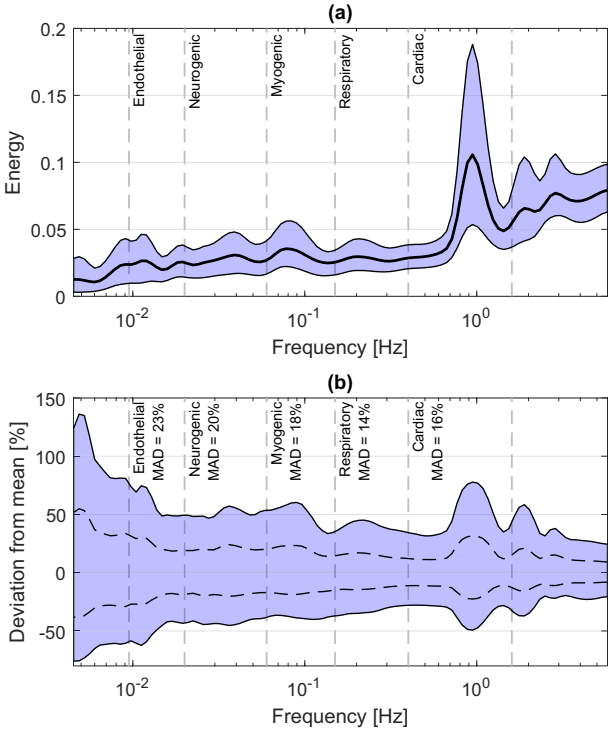

Fig. 8. Spatial variations in time-averaged wavelet spectrum in the large, dashed region of interest (ROI) (Fig. 3). (a) Time-averaged spectra in the ROI. The shaded area marks the 2.5th to the 97.5th percentile range, and the thick black line shows the mean of all spectra in the large ROI ($N = 36{,}775$). (b) Relative deviation from mean line in (a). The shaded area marks the 2.5th to the 97.5th percentile range and the dashed lines shows the mean deviation. The mean absolute deviation (MAD) in each frequency interval is also shown.

the affected images have been suggested (Lertsakdadet et al., 2018). However, in order to allow the use of frequency transforms, these samples must instead be replaced with synthetic data. The algorithm presented here for removing motion artifacts was designed based on empirical observations of the data, and further optimized using a large number of randomly generated synthetic perfusion signals. As seen in the example in Fig. 2, the energy from the motion artifact is drastically reduced, which allowed further analysis of the data. The choice to linearly interpolate the samples removed in the motion artifact detection was made to reduce the amount of false energy added by the synthetic data. Replacing the outliers with zeros would create discontinuities in the perfusion signal that, like the original motion artifacts, would contain high energy across the frequency spectrum. While there might be other interpolation methods that would further decrease the impact of the added synthetic data, the chosen linear interpolation was deemed the most robust based on our empirical tests. The suggested method works well for movement artifacts that are short in time. Artifacts that are longer than the period of the flowmotion waves, i.e. the inverse of the frequency, will drastically affect the calculated flowmotion energy. Measurements containing such long movement artifacts should thus be excluded.

The data analyzed in this paper was obtained by our MELSCI-based perfusion method described in previous papers (Fredriksson et al., 2019; Hultman et al., 2020). As already mentioned, this method is more accurate (linear) with respect to true perfusion and less noisy than current single-exposure LSCI methods. However, LSCI is currently the more common technique. We therefore also presented the results analyzed by single-exposure LSCI, to gauge viability of the proposed method in this case. To clarify, this analysis was made using the same data as the MELSCI-based results, by selecting a single exposure-time from the already acquired multi-exposure data. As such, we cannot say how currently available LSCI systems would perform in terms of noise levels, we can only evaluate the perfusion model used in some of these systems (Eq. (4)). Regardless, it is clear from Figs. 5 and 6 that LSCI is significantly less sensitive to cardiac activity. This can be seen both in the flowmotion image of cardiac activity (compare Figs. 3 and 5), as well as in the frequency spectrum of the two ROIs (compare Figs. 4 and 6). In the cardiac image in Fig. 3 (MELSCI-based), and to a lesser extent in the respiratory image in the same figure, a pattern of large vessels is visible. This pattern is entirely missing from the same images in Fig. 5 (LSCI-based). The cardiac peak in the frequency spectrum is also significantly lower in Fig. 6 (LSCI-based) compared to Fig. 4 (MELSCI-based). This is not unexpected given that LSCI underestimates high perfusion (Fredriksson and Larsson, 2016; Fredriksson et al., 2019; Tew et al., 2011; Binzoni et al., 2013; Humeau-Heurtier et al., 2013), and thus should be less sensitive to the flow in large vessels. More importantly however, the energies in the three lowest frequency bands – corresponding to the myogenic, neurogenic, and endothelial variations – are more comparable between MELSCI and LSCI. Although flowmotion has not yet reached clinical practice, all three of these frequency bands have shown potential importance to several pathological conditions (Rossi et al., 2008a) such as microvascular complications of type 2 diabetes (Reynès et al., 2021a; Los-Stegienta et al., 2021), rheumatological diseases (Mizeva et al., 2017), peripheral arterial disease (Rossi et al., 2005), critical ischemia (Anvar et al., 2000), and arterial hypertension (Rossi et al., 2006b; Bruning et al., 2015). This indicates clinical potential in both MELSCI-based and LSCI-based flowmotion analysis, despite the shortcomings of the latter. The clinical benefits of spatial analysis of flowmotion are still not clear but could potentially be a tool for assessment of skin function in applications such as burn injuries, skin infections, and free flaps, where the important information would be located in the transition from healthy to affected skin. Another potential area of interest is in sepsis, which is characterized by a heterogeneous degradation in endothelial microcirculatory function (Ince et al., 2016; Goldman et al., 2006), thus flowmotion imaging might present a direct method for monitoring the progression of the inflammation.

The wavelet transform provides time-localized information about the frequency content of the signal. As presented in Fig. 4 (CWT scalograms) and Fig. 9 (time-varying flowmotion images), this reveals another dynamic aspect of the data. The temporal variations in flowmotion might be indicative of the ability of the microvasculature to change how it regulates blood flow depending on tissue needs. In particular, the temporal peaks of the flowmotion signal might be of interest as an indicator of maximum activation capacity. Future studies should consider investigating the temporal peaks in flowmotion as a potential source of information in addition to the average energy.

Recording time is a central aspect when performing frequency analysis. The accuracy of the energy estimation of a certain frequency is related to the number of periods that fits into the recording. In this study, a recording time of 10 min was used. Thus, only about six periods of the lowest frequency band (0.0095–0.02 Hz) fits into the recording, while it has been suggested that the recording time should allow for at least 10 oscillations of the lowest analyzed frequency (Stefanovska, 1999). However, when applying spatial averaging of flowmotion videos it might not be necessary to extend the recording time for a sufficient accuracy. Our results indicate that there is a substantial spatial difference in the flowmotion activity. It appears that the flowmotion activity over time differs between tissue areas in an uncorrelated way (see Fig. 9 where image series for the various frequency bands are presented). Consequently, taking a spatial average will result in taking an average over multiple uncorrelated realizations of the same vasomotion process. It is likely that this will have at least a similar effect as averaging over a longer time-period. This should be investigated in future studies to possibly reduce the required recording time.

It has been proposed to analyze an even lower frequency band, 0.005–0.0095 Hz, that correlates to NO-independent endothelial activity (Kvandal et al., 2006; Bandrivskyy et al., 2004; Bagno and Martini,

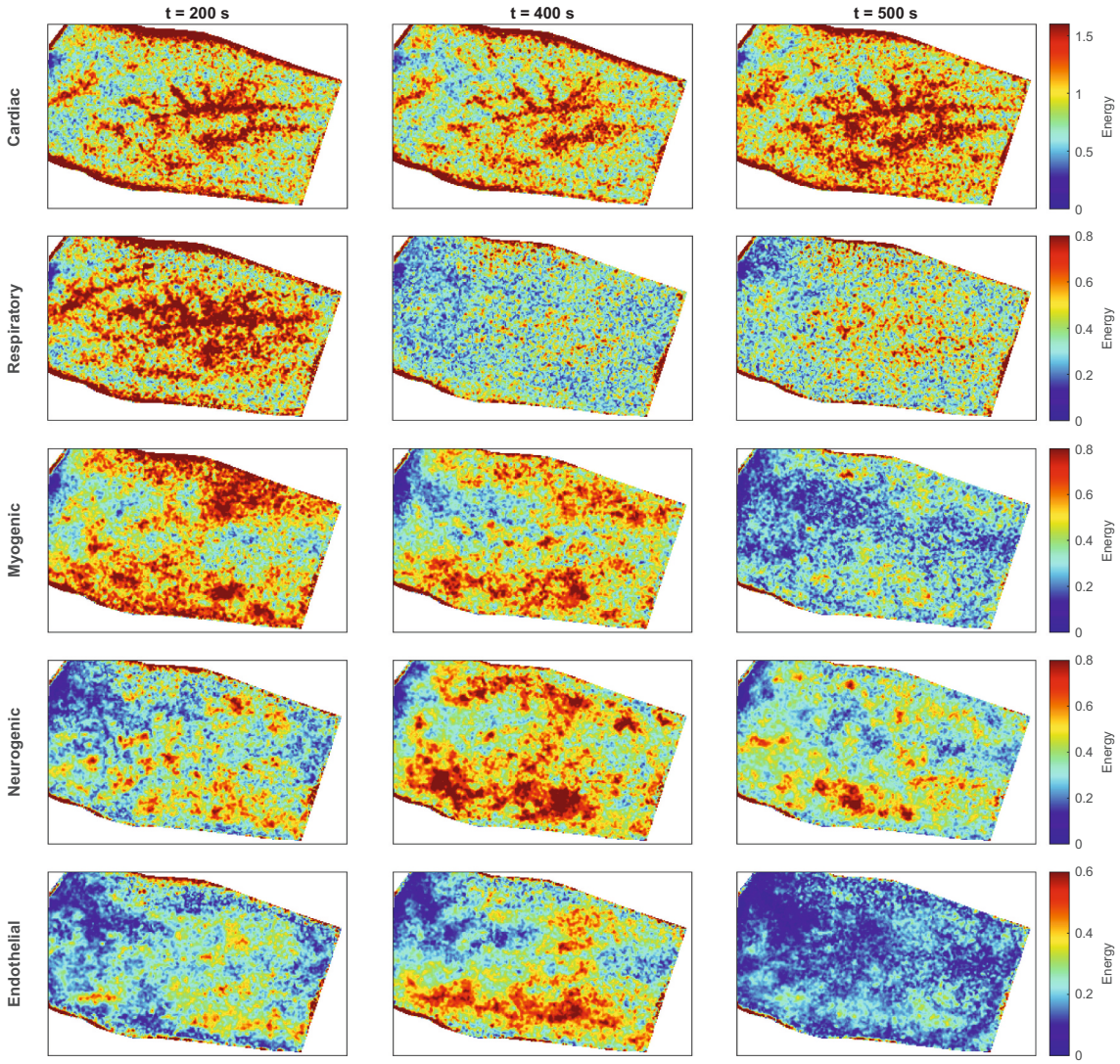

Fig. 9. Example of time-varying flowmotion activity. Flowmotion energy in each vasoregulatory process changes over time. The changes are not synchronous between the processes.

2015; Reynès et al., 2021b). Due to the recording time of 10 min, which only allows for three oscillations with 0.005 Hz, we have chosen not to specifically analyze that frequency band in this study, although it would be feasible with the technique as such. In future studies, the recording time is an important aspect to consider, where a longer recording time enable analysis of this NO-independent endothelial interval and general higher accuracy of the acquired energies. However, that should be balanced against other practical aspects such as increased risk of severe motion artifacts.

Since flowmotion analysis obtains information related to the regulatory mechanisms of the vasculature from baseline measurements, this implies that provocations might not be required to obtain clinically useful data. A few clinical studies have indeed found that certain pathological conditions cause basally reduced activity in one or more frequency bands, such as in patients with obesity (de Jongh et al., 2008), chronic renal failure (Stewart et al., 2004), or critical ischemia (Anvar et al., 2000). However, other studies have found that provocations are needed to elicit a difference in the measured flowmotion between the diseased and control groups. Examples of such provocations are arterial occlusion-release (Rossi et al., 2005; Rossi et al., 2007; Rossi et al., 2008b), iontophoresis of acetylcholine and sodium nitroprusside (Rossi et al., 2008c; Rossi et al., 2009; Schmiedel et al., 2007), local heating (Stewart et al., 2004; Rossi et al., 2009), and local pressure (Humeau et al., 2004). From a clinical perspective, provocation-free measurement protocols have many advantages. It is possible that the addition of spatial information gained by flowmotion imaging could lead to more applications in which basal changes are statistically significant, thus improving the clinical ease of use. Furthermore, the above clinical studies have only investigated the statistical differences between groups, not individuals. While there is value in understanding the differences between healthy and diseased groups, enabling individual diagnosis should be the ultimate goal of the technique. Because of the high heterogeneity in the microcirculation, this will likely only be possible using flowmotion imaging where the spatial variations can be accounted for.

5. Conclusion

In this paper we present a method for flowmotion imaging and show that the spatial variation in the microcirculation can lead to large uncertainties when using single-point measurement techniques. Future work should therefore strive to use imaging techniques to improve the ability to differentiate natural skin spatial variations from underlying pathological changes. We also observed interesting spatiotemporal patterns in the flowmotion, with yet unknown etiology, that could facilitate further clinical conclusions.

CRediT authorship contribution statement

Martin Hultman: Conceptualization, Methodology, Software, Validation, Formal analysis, Investigation, Writing – original draft, Writing – review & editing, Visualization. **Marcus Larsson:** Conceptualization, Methodology, Writing – review & editing. **Tomas Strömberg:** Conceptualization, Methodology, Resources, Writing – review & editing, Supervision, Funding acquisition. **Joakim Henricson:** Conceptualization, Methodology, Investigation, Resources, Writing – review & editing. **Fredrik Iredahl:** Conceptualization, Methodology, Resources, Writing – review & editing, Project administration, Funding acquisition. **Ingemar Fredriksson:** Conceptualization, Methodology, Software, Resources, Writing – review & editing, Supervision, Project administration, Funding acquisition.

Declaration of competing interest

Dr. Hultman and Dr. Fredriksson are part-time employed by Perimed AB, which is developing products related to research described in this publication.

Data availability

Data will be made available on request.

Acknowledgements

This study was financially supported by Sweden's Innovation Agency VINNOVA via the programs Swelife and MedTech4Health (Grant no. 2019-01522), by The Swedish Society of Medicine (SLS-961560), and by the Swedish state under the agreement between the Swedish government and the county councils, the ALF-agreement (RÖ-960844).

Appendix A. Supplementary data

Supplementary data to this article can be found online at https://doi.org/10.1016/j.mvr.2022.104456.

References

Anvar, M.D., et al., 2000. Patterns of skin flowmotion in the lower limbs of patients with chronic critical limb ischaemia (CLI) and oedema. Eur. J. Vasc. Endovasc. Surg. 20 (6), 536–544.
Bagno, A., Martini, R., 2015. Wavelet analysis of the Laser Doppler signal to assess skin perfusion. In: 2015 37th Annual International Conference of the IEEE Engineering in Medicine and Biology Society (EMBC).
Bandrivskyy, A., et al., 2004. Wavelet phase coherence analysis: application to skin temperature and blood flow. Cardiovasc. Eng. 4 (1), 89–93.
Binzoni, T., et al., 2013. Blood perfusion values of laser speckle contrast imaging and laser Doppler flowmetry: is a direct comparison possible? IEEE Trans. Biomed. Eng. 60 (5), 1259–1265.
Bračič, M., Stefanovska, A., 1998. Wavelet-based analysis of human blood-flow dynamics. Bull. Math. Biol. 60 (5), 919–935.
Bruning, R.S., Kenney, W.L., Alexander, L.M., 2015. Altered skin flowmotion in hypertensive humans. Microvasc. Res. 97, 81–87.
Clough, G.F., Kuliga, K.Z., Chipperfield, A.J., 2017. Flow motion dynamics of microvascular blood flow and oxygenation: evidence of adaptive changes in obesity and type 2 diabetes mellitus/insulin resistance. Microcirculation 24 (2), e12331.
Ellis, C.G., Jagger, J., Sharpe, M., 2005. The microcirculation as a functional system. Crit Care 9 Suppl 4 (Suppl. 4) p. S3-8.
Fredriksson, I., Larsson, M., 2016. On the equivalence and differences between laser Doppler flowmetry and laser speckle contrast analysis. Journal of Biomedical Optics 21 (12), p. 126018-126018.
Fredriksson, I., et al., 2019. Machine learning in multiexposure laser speckle contrast imaging can replace conventional laser Doppler flowmetry. J. Biomed. Opt. 24 (1).
Fredriksson, I., et al., 2022. Vasomotion analysis of speed resolved perfusion, oxygen saturation, red blood cell tissue fraction, and vessel diameter: novel microvascular perspectives. Skin Res. Technol. 28 (1), 142–152.
Goldman, D., Bateman, R.M., Ellis, C.G., 2006. Effect of decreased O2 supply on skeletal muscle oxygenation and O2 consumption during sepsis: role of heterogeneous capillary spacing and blood flow. Am. J. Phys. Heart Circ. Phys. 290 (6), H2277–H2285.
Hultman, M., et al., 2017. A 15.6 frames per second 1-megapixel multiple exposure laser speckle contrast imaging setup. J. Biophotonics 11 (2).
Hultman, M., et al., 2020. Real-time video-rate perfusion imaging using multi-exposure laser speckle contrast imaging and machine learning. J. Biomed. Opt. 25 (11), 1–15.
Humeau, A., et al., 2004. Spectral components of laser doppler flowmetry signals recorded in healthy and type 1 diabetic subjects at rest and during a local and progressive cutaneous pressure application: scalogram analyses. Phys. Med. Biol. 49 (17), 3957–3970.
Humeau-Heurtier, A., et al., 2013. Skin perfusion evaluation between laser speckle contrast imaging and laser Doppler flowmetry. Opt. Commun. 291, 482–487.
Ince, C., et al., 2016. The endothelium in sepsis. Shock 45 (3), 259–270.
de Jongh, R.T., et al., 2008. Impaired local microvascular vasodilatory effects of insulin and reduced skin microvascular vasomotion in obese women. Microvasc. Res. 75 (2), 256–262.
Kvandal, P., et al., 2006. Low-frequency oscillations of the laser Doppler perfusion signal in human skin. Microvasc. Res. 72 (3), 120–127.
Lertsakdadet, B., et al., 2018. Correcting for motion artifact in handheld laser speckle images. J. Biomed. Opt. 23 (3), 1–7.
Los-Stegienta, A., et al., 2021. Differentiation of diabetic foot ulcers based on stimulation of myogenic oscillations by transient ischemia. Vasc. Health Risk Manag. 17, 145–152.
Mizeva, I., et al., 2017. Analysis of skin blood microflow oscillations in patients with rheumatic diseases. J. Biomed. Opt. 22 (7), 070501.
Mizeva, I., et al., 2020. Wavelet analysis of the temporal dynamics of the laser speckle contrast in human skin. IEEE Trans. Biomed. Eng. 67 (7), 1882–1889.
Mizeva, I., et al., 2021. Spatial heterogeneity of cutaneous blood flow respiratory-related oscillations quantified via laser speckle contrast imaging. PLoS ONE 16 (5), e0252296.
Reynès, C., et al., 2021. Concomitant peripheral neuropathy and type 2 diabetes impairs postexercise cutaneous perfusion and flowmotion. J. Clin. Endocrinol. Metab. 106 (10), e3979–e3989.
Reynès, C., et al., 2021. Mechanisms of venoarteriolar reflex in type 2 diabetes with or without peripheral neuropathy. Biology (Basel) 10 (4).
Rossi, M., et al., 2005. Generalised wavelet analysis of cutaneous flowmotion during post-occlusive reactive hyperaemia in patients with peripheral arterial obstructive disease. Biomed. Pharmacother. 59 (5), 233–239.
Rossi, M., et al., 2006. The investigation of skin blood flowmotion: a new approach to study the microcirculatory impairment in vascular diseases? Biomed. Pharmacother. 60 (8), 437–442.
Rossi, M., et al., 2006. Spectral analysis of laser doppler skin blood flow oscillations in human essential arterial hypertension. Microvasc. Res. 72 (1–2), 34–41.
Rossi, M., et al., 2007. Absent post-ischemic increase of blood flowmotion in the cutaneous microcirculation of healthy chronic cigarette smokers. Clin. Hemorheol. Microcirc. 36 (2), 163–171.
Rossi, M., et al., 2008. Skin vasomotion investigation: a useful tool for clinical evaluation of microvascular endothelial function? Biomed. Pharmacother. 62 (8), 541–545.
Rossi, M., et al., 2008. Blunted post-ischemic increase of the endothelial skin blood flowmotion component as early sign of endothelial dysfunction in chronic kidney disease patients. Microvasc. Res. 75 (3), 315–322.
Rossi, M., et al., 2008. Blunted increase of digital skin vasomotion following acetylcholine and sodium nitroprusside iontophoresis in systemic sclerosis patients. Rheumatology (Oxford) 47 (7), 1012–1017.
Rossi, M., et al., 2009. Skin blood flowmotion and microvascular reactivity investigation in hypercholesterolemic patients without clinically manifest arterial diseases. Physiol. Res. 58 (1), 39–47.
Schmiedel, O., Schroeter, M.L., Harvey, J.N., 2007. Microalbuminuria in type 2 diabetes indicates impaired microvascular vasomotion and perfusion. Am. J. Physiol. Heart Circ. Physiol. 293 (6), H3424–H3431.
Stefanovska, A., 1999. Physics of the human cardiovascular system. Contemp. Phys. 40 (1), 31–55.
Stefanovska, A., Bracic, M., Kvernmo, H.D., 1999. Wavelet analysis of oscillations in the peripheral blood circulation measured by laser Doppler technique. IEEE Trans. Biomed. Eng. 46 (10), 1230–1239.
Stewart, J., et al., 2004. Noninvasive interrogation of microvasculature for signs of endothelial dysfunction in patients with chronic renal failure. Am. J. Physiol. Heart Circ. Physiol. 287 (6), H2687–H2696.
Tew, G.A., et al., 2011. Comparison of laser speckle contrast imaging with laser Doppler for assessing microvascular function. Microvasc. Res. 82 (3), 326–332.
Torrence, C., Compo, G.P., 1998. A practical guide to wavelet analysis. Bull. Am. Meteorol. Soc. 79 (1), 61–78.
Wardell, K., et al., 1994. Spatial heterogeneity in Normal skin perfusion recorded with laser Doppler imaging and flowmetry. Microvasc. Res. 48 (1), 26–38.